^{1}H-n.m.r. study of the solution properties and secondary structure of neurotoxin III from the sea anemone *Anemonia sulcata*

Raymond S. NORTON,*§ Keith CROSS,† Vijoleta BRAACH-MAKSVYTIS* and Elmar WACHTER‡

*School of Biochemistry, University of New South Wales, Kensington 2033, Australia, †NMR Unit, University of New South Wales, Kensington 2033, Australia, and ‡Institute of Physiological Chemistry, University of Münich, Germany

The solution properties, secondary structure and global fold of the 27-residue polypeptide neurotoxin III (ATX III), from the sea anemone *Anemonia sulcata*, have been investigated using high-resolution ^{1}H-n.m.r. spectroscopy. Studies of the concentration dependence of the n.m.r. spectrum indicate that the molecule self-associates in the millimolar concentration range useable for n.m.r. analysis, the association being less pronounced at acidic pH values. The dependence on pH of association implies that electrostatic interactions play a role in this process, while the significant concentration-dependent shifts of the aromatic resonances of Tyr-7 and Trp-13 indicate that hydrophobic interactions also contribute. Individual pK_a values have been determined for most ionizable groups in the molecule. Sequence-specific resonance assignments were obtained for all protons using a range of two-dimensional homonuclear-correlated and nuclear-Overhauser-effect (nOe) spectra. The secondary structure of the polypeptide was identified from sequential (i, $i+1$) and medium-range (i, $i+2/3/4$) nOe connectivities, NH to $C^\alpha H$ coupling constants, $C^\alpha H$ chemical shifts, and the location of slowly exchanging backbone-amide protons. ATX III contains no regular α-helix or β-sheet, consisting instead of a network of reverse turns. nOe conectivities between half-cystine residues are consistent with the disulphide pairings 3–17, 4–11 and 6–22. ATX III has a well-defined structure and appears to lack the disordered loop which, in the longer sea anemone toxins (46–49 residues), may be part of the receptor-binding surface.

INTRODUCTION

Sea anemones express a variety of polypeptide and protein toxins, many of which are important components of the venom used by these animals for both defence and the capture of prey (Beress, 1982; Kem, 1988). The best characterized of these toxins are the 5000 Da proteins that act by binding to the voltage-gated sodium channels of excitable tissue (Catterall, 1988). On the basis of their amino-acid sequences and immunological cross-reactivity, these proteins have been classified into two groups, designated types 1 and 2 (Kem, 1988; Norton, 1991). Three-dimensional structures have been determined for four of these proteins, two from the first group (Torda et al., 1988; Widmer et al., 1989) and two from the second (Fogh et al., 1990; Kumar et al., 1990), and progress is being made towards an understanding of their structure–function relationships (Barhanin et al., 1981; Gould et al., 1990; Norton, 1991). Both within and between the two groups of toxins there is a considerable range of tissue and species specificity, some being very potent neuro- and cardiotoxins in mammals, others being essentially crustacean-specific.

The sodium-channel-binding sites for the two groups of toxins are thought to be identical, or very similar, but little is known about the structure of the binding site or the nature of the interactions between the toxins and the channel. Because of the complexity of the sodium-channel molecule, the best prospect for establishing a model of this interaction in the near future lies in characterizing the receptor-binding surface of the toxins themselves. This will come primarily from detailed studies of the three-dimensional structures and structure–function relationships of the toxins, but will also benefit from information derived from other proteins that bind to the same receptor site. In this context it is noteworthy that the α-scorpion toxins and the sea anemone polypeptides BDS I and BDS II appear to bind to the same receptor site (Catterall, 1988; Llewellyn and Norton, 1991). Three-dimensional structures have been determined for these proteins (Fontecilla-Camps et al., 1988; Driscoll et al., 1989) and some information has been deduced about their receptor-binding surfaces.

Another class of molecule that appears to bind to the same site is the short sea anemone polypeptides, represented by *Anemonia sulcata* neurotoxin III (ATX III) (Beress et al., 1975) and *Parasicyonis actinostoloides* toxin (Nishida et al., 1985). The former contains 27 residues and three disulphide bonds, the latter 31 residues and four disulphide bonds. There is distinct amino-acid-sequence identity between these two molecules, but almost none with the longer proteins of types 1 and 2. The fact that these short polypeptides appear to bind to the same receptor site on the sodium channel, while having negligible sequence similarity, provides a strong incentive for determining their three-dimensional structures. This is strengthened by the finding that antibodies raised against ATX III are able to neutralize the effects of intracerebroventricular injection of one of the long polypeptides (Bahraoui et al., 1989), suggesting that antigenic determinants shared by the short and long polypeptides overlap the site responsible for biological activity. As there is no X-ray crystal structure available for the short polypeptides, and as they are of a size well-suited to n.m.r. studies (Wüthrich, 1986; Norton, 1990), we have undertaken a study of the structure and properties of ATX III in solution using this approach. In this paper we describe the solution properties, sequence-specific

Abbreviations used: ATX III, *Anemonia sulcata* neurotoxin III; DQF-COSY, double-quantum-filtered two-dimensional scalar correlated spectroscopy; DQ, two-dimensional double quantum coherence spectroscopy; HOHAHA, two-dimensional homonuclear–Hartmann–Hahn spectroscopy; nOe, nuclear Overhauser effect; NOESY, two-dimensional dipolar correlated spectroscopy.

§ To whom correspondence should be addressed at: NMR Laboratory, Biomolecular Research Institute, 381 Royal Parade, Parkville, Victoria 3052, Australia.

resonance assignments, secondary structure and overall topology of the molecule.

MATERIALS AND METHODS

Materials

Initial n.m.r. studies were carried out on ATX III purified from the sea anemone *Anemonia sulcata* as described by Beress et al. (1975). Analysis of this material by reverse-phase h.p.l.c. showed that it contained protein impurities. Before the two-dimensional n.m.r. experiments used for resonance assignments were performed these impurities were removed by reverse-phase h.p.l.c. on a Vydac reverse-phase C-18 column using water and acetonitrile eluants, each containing 0.1% trifluoroacetic acid. For some n.m.r. experiments, labile protons were exchanged with deuterium by incubation of the protein in ^2H_2O (> 99.75% ^2H, from the Australian Atomic Energy Commission, Lucas Heights, NSW, Australia) at room temperature, followed by lyophilization. Protein concentrations for two-dimensional n.m.r. experiments were in the range 2–5 mM and a pH value of 2.5 was used to minimize the effects of self-association (see the Results section).

N.m.r. spectroscopy

Most one-dimensional n.m.r. spectra were recorded at 300.07 MHz on a Bruker CXP-300 spectrometer operating in the pulsed Fourier transform mode with quadrature detection. With the exception of some preliminary spectra at 300 MHz, all two-dimensional n.m.r. spectra were recorded at 500.14 MHz on an AM-500 spectrometer equipped with an Aspect 3000 computer and process controller. All experiments were carried out at 27 °C unless otherwise noted. The carrier was set in the centre of the spectrum, and quadrature detection was used in both dimensions. All two-dimensional spectra were recorded in phase-sensitive mode by using the time-proportional phase incrementation method (Marion and Wüthrich, 1983). Two-dimensional dipolar correlated spectroscopy (NOESY) spectra (Jeener et al., 1979; Macura et al., 1981) were recorded for samples in ^2H_2O or 90% H_2O/10% ^2H_2O with mixing times in the range 100–250 ms. Double-quantum-filtered two-dimensional scalar correlated spectroscopy (DQF-COSY) experiments (Piantini et al., 1982; Shaka and Freeman, 1983) were acquired by using $90°_x90°_y$ composite 90° pulses according to Müller et al. (1986). Two-dimensional homonuclear–Hartmann–Hahn spectroscopy (HOHAHA) spin lock experiments using the MLEV-17 sequence (Braunschweiler and Ernst, 1983; Bax and Davis, 1985) were recorded with mixing times of 50 or 80 ms. To assign slowly exchanging backbone-amide protons, a HOHAHA experiment with a mixing time of 80 ms was carried out at 27 °C on a fully protonated sample of ATX III immediately after its dissolution in ^2H_2O (final pH 2.6). A two-dimensional double quantum coherence spectroscopy (DQ) experiment (Wokaun and Ernst, 1977; Wagner and Zuiderweg, 1983), with a preparation time of 46 ms, was performed on the sample in H_2O. A $90°_x180°_y90°_x$ composite 180° pulse (Levitt and Freeman, 1979) was used for refocusing.

Solvent suppression was carried out by selective, low-power irradiation of the water resonance during the relaxation delay, which was typically 2.0 s. Spectral widths were 5700–6000 Hz for samples in H_2O and 5400 Hz for ^2H_2O, acquired over 4K data points. Typically, 270–500 t_1 increments were acquired, with 64–128 scans per increment. Spectra were processed either on the Aspect 3000 computer using DISNMR or on IRIS 4D/20 and IRIS 4D/30 workstations using FELIX version 1.1 (Hare Research Inc., Bothell, WA, U.S.A.). Spectra processed in FELIX were subjected to baseline correction and t_1 noise suppression as described by Manoleras and Norton (1992). Before Fourier transformation, phase-shifted, sine or sine-squared window functions were applied, with phase shifts of 45–60° in ω_1 and 30–60° in ω_2. Final matrix sizes were usually 2K × 2K real points, with 4K real points in ω_2 being used in some cases. Spectra are presented as contour plots with no distinction between positive and negative peaks and with successive plotting levels differing by a factor of 1.4.

Chemical shifts were measured using 1,4-dioxan, at 3.751 p.p.m. downfield from 2,2-dimethyl-2-silapentane-5-sulphonate, as internal standard. The pH values are uncorrected meter readings made at room temperature. Probe temperature was calibrated using methanol and ethylene glycol (van Geet, 1970). pK_a values were obtained by non-linear least-squares fits of the observed chemical shifts expressed as a function of pH to the Henderson–Hasselbalch equation for a single ionization, assuming fast exchange between the conjugate acids and bases. Backbone-amide exchange rates were measured from a series of one-dimensional spectra at 300 MHz recorded at various times after dissolution of normal isotopic ATX III in ^2H_2O at pH 2.8 and 27 °C. Exchange rates were estimated from peak heights assuming first-order kinetics.

RESULTS

Initial one-dimensional n.m.r. experiments on ATX III revealed a marked concentration dependence of the chemical shifts of a number of resonances in the spectrum. This section therefore commences with a description of the pH- and concentration-dependence of the spectrum of ATX III, the result of which were used in the choice of suitable solution conditions for subsequent two-dimensional n.m.r. experiments. Resonance assignments described later are assumed in interpreting the one-dimensional spectra.

Effects of ATX III concentration and pH

Figure 1 shows the aromatic region of one-dimensional spectra of ATX III at protein concentrations in the range 0.3–5.1 mM in ^2H_2O at pH 4.1 and 27 °C. Clearly some resonances are markedly concentration dependent, while others are largely unaffected. Results for the aromatic resonances of the two tyrosine residues at pH values of 2.0, 4.1 and 6.1 are summarized in Figure 2. Two trends are evident, the first being that the aromatic resonances of Tyr-7 are strongly concentration dependent while those of Tyr-18 are essentially independent, and the second that the concentration dependence is less severe at a pH value of 2 than at higher pH values. Aromatic resonances from both tryptophan residues are affected, although the effects on Trp-13 are greater than those on Trp-8 and neither is affected to the same degree as Tyr-7. In the upfield region of the spectrum the highly shifted $C^\beta H$ resonance of Cys-11 at 0.14 p.p.m. is also markedly concentration dependent. The backbone-amide resonances of Tyr-7, Cys-11, Trp-13 and Gly-14 are all shifted upfield by 1.7–2.0 p.p.m. from their expected positions in unstructured peptides. These perturbations must arise, in part, from aromatic-ring current shifts (Wüthrich, 1986) and reflect a local environment rich in aromatic character, either in the monomer, or the associated protein, or both. The only side-chain resonances to be strongly perturbed are those of Cys-11.

ATX III contains relatively few ionizable groups, made up of the side-chains of Glu-20, Tyr-7, Tyr-18 and Lys-26, in addition to the N- and C-termini. The effects of pH on well-resolved

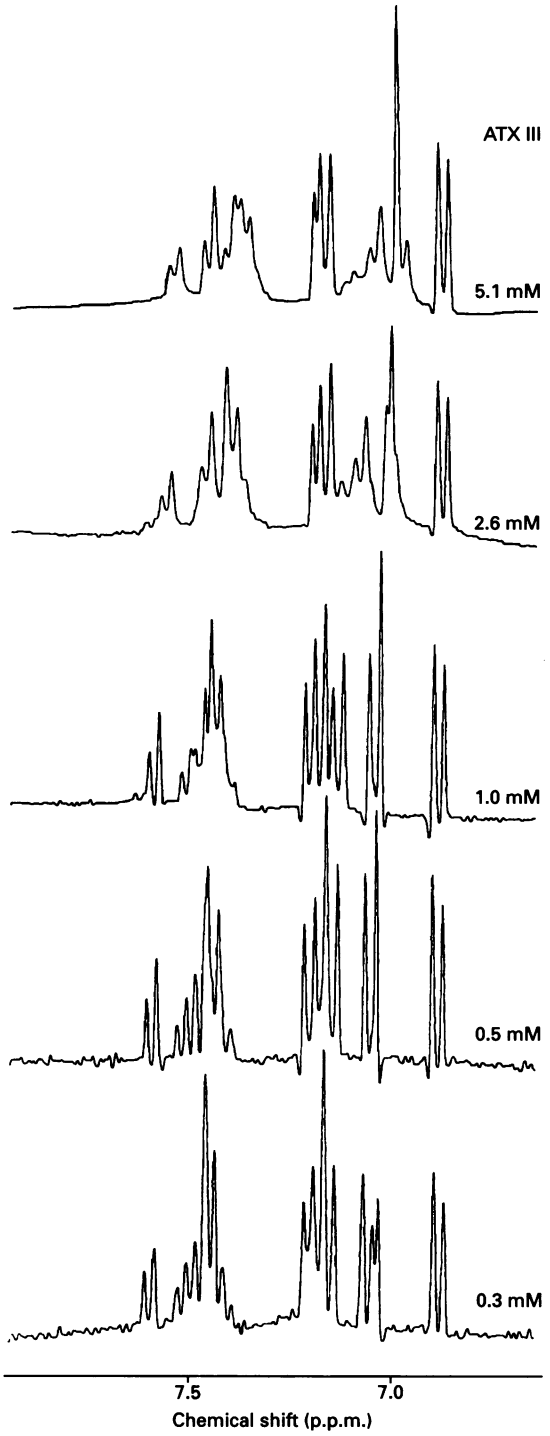

Figure 1 Aromatic region of one-dimensional ^{1}H-n.m.r. spectra, recorded at 300 MHz, of ATX III in ^2H_2O at pH 4.1 and 27 °C over the concentration range 0.3–5.1 mM

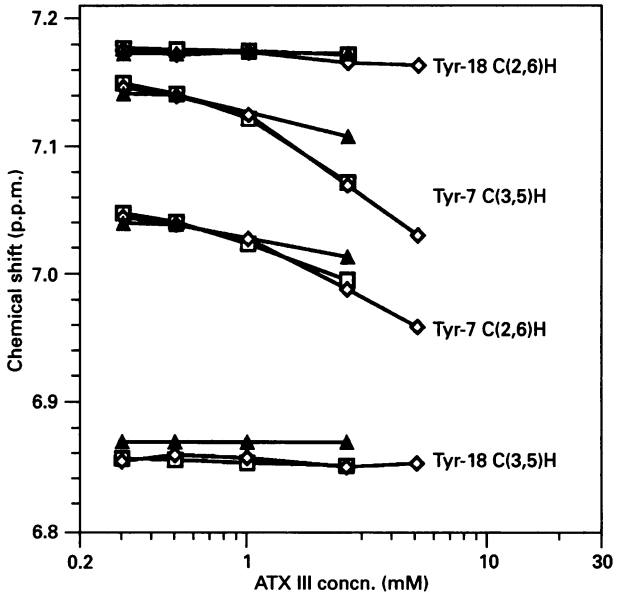

Figure 2 Concentration dependence on the chemical shifts of tyrosine aromatic proton resonances of ATX III in ^2H_2O at 27 °C

Data at pH 2.0 are represented by closed triangles, at pH 4.1 by open diamonds, and at pH 6.1 by open squares.

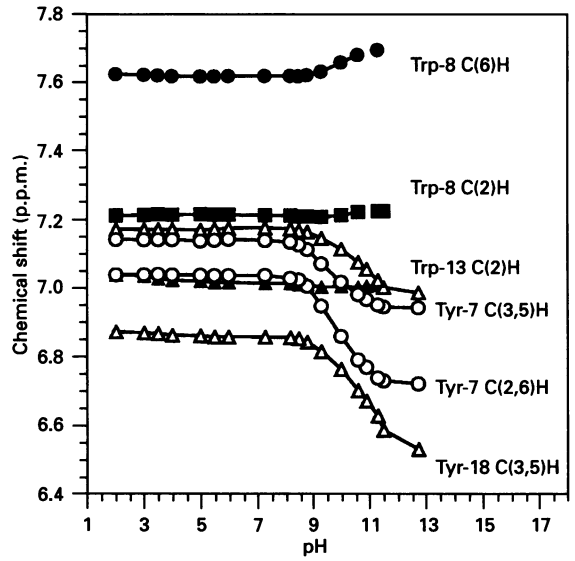

Figure 3 pH dependence of the chemical shifts of aromatic proton resonances of ATX III in ^2H_2O at 27 °C

For clarity, the graph for the C(2,6)H resonance of Tyr-18 (open triangles) is not labelled.

resonances in the aromatic region of the spectrum are illustrated in Figure 3 and the pK_a values derived from these resonances, as well as some in the aliphatic region of the spectrum, are summarized in Table 1.

Titration of the N-terminal ammonium group is reflected in a 0.05 p.p.m. upfield shift of the $C^\delta H_2$ resonance of Arg-1 with a pK_a value of approx. 7.4; however, peak overlap in spectra at pH values of 6–7 prevents a more accurate definition of this pK_a. The phenolic pK_a value of Tyr-18, 10.1, is very close to that found in small peptides (Bundi and Wüthrich, 1979), suggesting that the aromatic ring is not involved in strong interactions with surrounding residues. Its chemical shifts are also unaffected by aggregation. The phenolic pK_a of Tyr-7 is only slightly perturbed, but the chemical shifts of its aromatic proton resonances are inverted relative to those in small peptides, as are the magnitudes of their titration shifts (Table 1). The aromatic resonances of Tyr-7 are strongly affected by aggregation. It is interesting to

Table 1 Titration behaviour of residues in ATX III in ^2H_2O at 0.5 mM and 27 °C

Data were obtained from one-dimensional spectra recorded at 300 MHz. δ_A and δ_B are limiting chemical shifts at the acidic and basic extremes of the titration to which the pK_a refers. pK_a values were determined from non-linear least-squares fits to the equation for a single ionization; S.D. values are given in parentheses.

Residue	Resonance observed	δ_A	$\delta_A-\delta_B$	pK_a (S.D.)
Tyr-7	C(2,6)H	7.02	0.29	9.7 (0.2)
	C(3,5)H	7.13	0.18	9.8 (0.1)
Trp-8	C(2)H	7.21	−0.02	10.1 (0.2)
	C(4)H	7.62	−0.08	10.1 (0.3)
Cys-11	$C^{\alpha}H$	2.68	0.01	5.4 (0.2)
		2.67	−0.03	11.3 (0.5)
	$C^{\beta}H$	0.20	−0.03	10.1 (0.3)
Trp-13	C(2)H	7.04	0.02	3.4 (0.2)
Gly-14	$C^{\alpha}H$	3.15	0.02	3.2 (0.2)
Tyr-18	C(2,6)H	7.17	0.15	10.1 (0.2)
	C(3,5)H	6.87	0.01	3.5 (0.3)
		6.85	0.23	10.1 (0.2)
Gly-24	$C^{\alpha}H$	3.82	0.01	10.1 (0.3)
Val-27	$C^{\gamma}H_3$	0.79	0.05	3.3 (0.3)
		0.75	−0.01	5.4 (0.2)
		0.76	−0.02	11.3 (0.4)
	$C^{\gamma}H_3$	0.84	0.02	3.3 (0.2)
		0.82	−0.01	5.3 (0.3)

note that the aromatic resonances of Trp-8 are more affected by the phenolic pK_a of Tyr-18 than that of Tyr-7. Resonances from a number of residues, most notably those of Val-27, sense titration of a carboxyl group with a pK_a value of 3.3, which is most probably the C-terminus. The other carboxyl group in the molecule, the γ-carboxyl of Glu-20, appears to have a pK_a value of 5.4, as reflected in titration shifts of Cys-11 and Val-27. This is higher than the corresponding pK_a value in small peptides, consistent with involvement of this residue in a hydrophobic environment or proximity to a negative charge or both. Support for the second possibility comes from the observation that resonances of Val-27, the only other residue in the molecule containing a negatively charged group, also sense the titration with pK_a 5.4. The pH titration was not extended to determine pK_a values for the remaining ionizable groups from Arg-1 and Lys-26.

The effects of aggregation on the resonances of Tyr-7 and Tyr-18 (Figure 2) and other residues (results not shown) are significantly greater at pH values of 4–6 than at pH 2. Taken together with the pK_a values described above, this suggests that electrostatic and/or hydrogen-bonding interactions involving the carboxylate form of the C-terminus contribute to aggregation. The potential partners in a purely electrostatic interaction are limited to Arg-1 and Lys-26.

On the basis of the above results, it was decided that resonance assignments would be made at a pH value of 2.5. Chemical shifts at this pH are still concentration dependent, but not to the extent that minor differences in sample concentration would cause uncertainty in assignments. Given that the overall conformation of the molecule (as reflected in its ^1H chemical shifts) is largely conserved between pH values of 2 and 7, determining the structure at low pH values appeared preferable to determining the structure of a more highly aggregated form at physiological pH values.

Sequence-specific resonance assignments

Resonances were assigned to specific protons in the molecule using a modified form of the sequential assignment procedure of

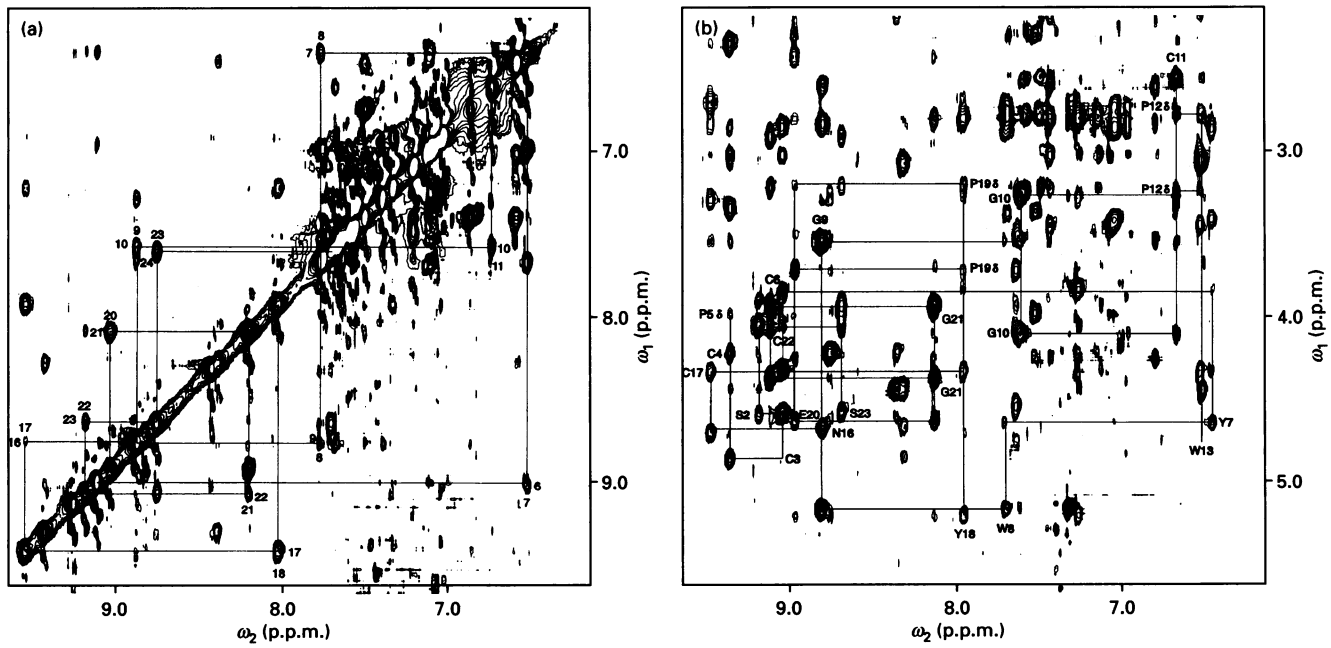

Figure 4 NOESY spectrum of 5 mM ATX III in 90% H_2O/10% ^2H_2O at pH 2.5 and 27 °C, recorded at 500 MHz with a 250-ms mixing time

(**a**) NH–NH region showing d_{NN} (i, $i+1$) connectivities for residues 6–11, 16–18 and 20–24. (**b**) NH–$C^{\alpha}H$ region showing $d_{\alpha N}$ (i, $i+1$) connectivities for residues 1–13 and 16–23. Intraresidue NH–$C^{\alpha}H$ cross-peaks are marked with the residue number. Connectivities from NH to proline $C^{\delta}H$ resonances are also shown.

Table 2 Chemical-shift values of ^{1}H resonances of ATX III in aqueous solution at pH 2.5 and 27 °C

Chemical-shift values are expressed in p.p.m. downfield from 2,2-dimethyl-2-silapentane-5-sulphonate (DSS). Estimated accuracy 0.02 p.p.m. For methylene groups, two chemical shifts are indicated only where both protons were assigned; a single entry indicates that it was not established whether the two resonances were degenerate.

Residue	NH	$C^{\alpha}H$	$C^{\beta}H$	Other
Arg-1	*	4.09	1.83, 1.91	$C^{\gamma}H_2$ 1.64, 1.72; $C^{\delta}H_2$ 3.05, 3.05; $N^{\epsilon}H$ 7.04
Ser-2	9.09	4.65	3.98, 4.11	
Cys-3	8.96	4.93	2.92, 3.09	
Cys-4	9.26	4.27	2.43, 3.41	
Pro-5	–	4.38	0.66, 2.13	$C^{\gamma}H_2$ 2.39; $C^{\delta}H_2$ 3.45, 4.05
Cys-6	8.96	3.90	1.72, 2.12	
Tyr-7	6.37	4.70	2.93, 3.47	C(2,6)H 6.94; C(3,5)H 7.06
Trp-8	7.61	5.23	2.80, 2.88	N(1)H 10.14; C(2)H 7.24; C(4)H 7.59; C(5)H 7.46; C(6)H 7.39; C(7)H 7.50
Gly-9	8.72	3.61, 3.61		
Gly-10	7.52	3.34, 4.16		
Cys-11	6.58	2.64	0.14, 2.09	
Pro-12	–	4.38	2.13, 2.40	$C^{\gamma}H_2$ 2.24; $C^{\delta}H_2$ 2.86, 3.29
Trp-13	6.43	4.87	3.10, 3.51	N(1)H 10.50; C(2)H 6.98; C(4)H 7.35; C(5)H 7.34; C(6)H 7.05; C(7)H 7.44
Gly-14	6.43	3.13, 4.49		
Gln-15	8.22	4.73	1.90	$C^{\gamma}H_2$ 2.17; $N^{\epsilon}H_2$ 6.90, 7.24
Asn-16	8.71	4.74	2.67, 2.91	$N^{\delta}H_2$ 6.70, 7.34
Cys-17	9.38	4.39	2.78, 3.36	
Tyr-18	7.87	5.27	2.80, 2.89	C(2,6)H 7.18; C(3,5)H 6.87
Pro-19	–	4.29	2.01, 2.28	$C^{\gamma}H_2$ 1.90, 1.94; $C^{\delta}H_2$ 3.27, 3.79
Glu-20	8.88	4.70	1.96, 1.96	$C^{\gamma}H_2$ 2.37, 2.50
Gly-21	8.04	4.00, 4.43		
Cys-22	9.03	4.13	2.98, 3.29	
Ser-23	8.61	4.64	3.94, 4.01	
Gly-24	7.55	3.78, 4.60		
Pro-25	–	4.49	1.82, 2.27	$C^{\gamma}H_2$ 1.93, 1.98; $C^{\delta}H_2$ 3.58
Lys-26	8.26	4.27	1.50, 1.63	$C^{\gamma}H_2$ 0.82, 1.20; $C^{\delta}H_2$ 1.52, 1.70; $C^{\epsilon}H_2$ 2.95, 2.95
Val-27	8.67	4.27	2.08	$C^{\gamma}H_3$ 0.79, 0.84

* Protons exchange with solvent too quickly to be observed under the present conditions.

Wüthrich and co-workers (Billeter et al., 1982; Wüthrich, 1986), in which extensive use was made of HOHAHA spectra of ATX III in H_2O to define complete amino-acid spin systems commencing at the backbone-amide proton (Chazin and Wright, 1987). As these methods are well-established, details of the assignment procedure will not be documented here; the range of two-dimensional n.m.r. experiments used is summarized in the Materials and methods section. The small size of the molecule, coupled with the presence of four aromatic residues, made the assignment procedure relatively straightforward, allowing a complete set of assignments to be obtained. The only problem was encountered at residues 13 and 14, where the NH chemical shifts are essentially identical and the $C^{\alpha}H$ resonance of Trp-14 was saturated by solvent irradiation. The DQ spectrum was valuable in assigning this region of the spectrum. Two regions of a NOESY spectrum showing nOe connectivities involving backbone-amide proton resonances are illustrated in Figure 4.

Table 2 gives the chemical-shift values of all resonances in ATX III and Figure 5 summarizes the types of sequential nOe connectivities (i, $i+1$) on which the specific assignments are based. Except where peak overlap prevents their observation, $d_{\alpha N}$ connectivities are found for all residue pairs, and in most cases are supported by d_{NN} and $d_{\beta N}$ connectivities. The conformation of all peptide bonds preceding proline residues appears to be *trans* based on the observation of strong $d_{\alpha\delta}(i, i+1)$ connectivities expected for this conformation (Arseniev et al., 1984). Also shown in Figure 5 are estimates of the three-bond NH to $C^{\alpha}H$ coupling constants (taken from one-dimensional spectra), the positions of slowly exchanging amide protons (cross-peaks from which were visible in a HOHAHA spectrum of partially exchanged ATX III) and the locations of medium-range nOe connectivities.

Estimates of the backbone-amide exchange rates were made from one-dimensional spectra at 300 MHz. Amides which are indicated as slowly exchanging in Figure 5 have k_m values of 0.0002–0.005 min^{-1}, while the three indicated as having intermediate exchange rates (which were visible in one-dimensional spectra before acquisition of the HOHAHA spectrum, but gave only very weak cross-peaks in the latter) have rates of 15×10^{-3}–25×10^{-3} min^{-1}.

Secondary structure and global fold

The results summarized in Figure 5 are not consistent with the presence of extensive regions of β-sheet or helix in ATX III. Helical regions are expected to have continuous stretches of strong $d_{NN}(i, i+1)$ nOe connectivities, small NH to $C^{\alpha}H$ coupling constants and slowly exchanging backbone-amide protons, as well as a network of medium-range connectivities [$d_{NN}(i, i+2)$, $d_{\alpha N}(i, i+3)$ and $d_{\alpha\beta}(i, i+3)$] (Wüthrich, 1986), criteria which are not collectively satisfied anywhere in the molecule. Regions of β-sheet are characterized by stretches of strong $d_{\alpha N}$ connectivities and large NH to $C^{\alpha}H$ coupling constants, together with a network of slowly exchanging backbone-amide protons and strong interstrand connectivities ($d_{\alpha\alpha}$, $d_{\alpha N}$ or d_{NN} depending on the type of sheet). On this basis, residues 13–19 have some features consistent with a β-sheet structure, but the presence of medium-range nOe connectivities overlapping with this region makes it unlikely that this structure is present. Rather, the presence of a large number of i to $i+2$ and i to $i+3$ connectivities,

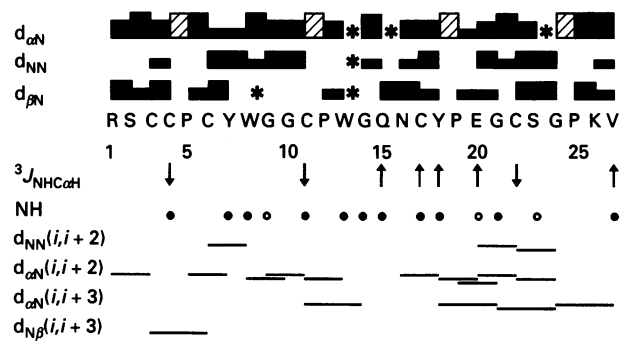

Figure 5 Summary of n.m.r. data used for sequence-specific assignments and the identification of secondary structure elements of ATX III

Filled bars indicate sequential connectivities observed in a 250-ms mixing time NOESY spectrum of ATX III in H_2O at pH 2.5 and 27 °C. The height of the bar indicates the strength of the nOe, categorized as strong, medium or weak. Shaded bars represent $d_{\alpha\delta}$ (i, $i+1$) connectivities to proline residues. Note that for all four proline residues at least one $d_{N\delta}$ ($i-1$, i) and one $d_{\beta N}$ (i, $i+1$) connectivity could also be observed, allowing continuous sequential assignments to be made from the fingerprint region of the spectrum. Connectivities that could not be identified because of peak degeneracy or overlap with the residual water resonance are indicated with asterisks (*). Values of $^3J_{HNC\alpha H}$ are indicated by ↓ if < 5.5 Hz and ↑ if > 8.5 Hz (except where peak overlap prevented their measurement). Slowly exchanging backbone amide protons (as defined by their presence in the exchange HOHAHA recorded at pH 2.6 and 27 °C) are indicated by closed circles in the row labelled NH. Open circles in the NH row denote amides with intermediate exchange rates, which were visible in one-dimensional spectra recorded before recording of the HOHAHA spectrum but gave very weak cross-peaks. Medium-range nOe connectivities are also shown, but in this case the height of the bars does not indicate the strength of the nOe.

most notably $d_{\alpha N}$ (i, $i+2$), coupled with the absence of continuous stretches of d_{NN} (i, $i+1$), implies that ATX III consists of a network of reverse turns.

Another useful indicator of ordered secondary structure is the $C^{\alpha}H$ chemical shift, with upfield shifts corresponding to helical regions and downfield shifts to extended, sheet-like regions (Wishart et al., 1992). Using these criteria, the $C^{\alpha}H$ chemical shifts in the spectrum of ATX III indicate the absence of α-helix or β-sheet, in agreement with the conclusions drawn from the pattern of nOe connectivities, coupling constants and slowly exchanging amide protons.

The structure of ATX III, therefore, consists of a network of reverse turns. As has been noted previously (Wüthrich, 1986), the exact identity and location of reverse turns can be difficult to specify using the type of data summarized in Figure 5 and this is best left until the stage of tertiary-structure determination. One problem in particular is that, because of their tendency to be located on protein surfaces, the hydrogen-bonded backbone amides in turns are not always slowly exchanging. In the case of ATX III the correlation of slowly exchanging backbone amides with $i+3$ residues in turns is complicated further by the possible contribution of aggregation to a reduction in certain exchange rates. Thus, while the data in Figure 5 are consistent with two turns in the region of residues 6 to 14 and two or three for residues 16 to 27, with an additional turn possible at the N-terminus, the exact locations of the turns are not specified at this stage.

An important factor in determining the global fold of ATX III is the location of the three disulphide bonds, which in this case have not been determined previously. In principle, the disulphide pairings could be determined from $C^{\beta}H$ to $C^{\beta}H$ nOe connectivities across the disulphide bonds, but in practice these can be rather weak and often occur in crowded regions of the spectrum. There is a weak nOe between the $C^{\beta}H$ resonances of Cys-4 and Cys-17. On the other hand, nOes are also observed between the Cys-11 $C^{\beta}H$ resonance at 0.14 p.p.m. and both $C^{\beta}H$ resonances of Cys-4, and $C^{\alpha}H$ to $C^{\beta}H$ nOes are observed from Cys-3 to Cys-17 and Cys-6 to Cys-22. These nOes are consistent with the disulphide pairings 3–17, 4–11 and 6–22, but confirmation of these pairings must await the complete structure determination.

DISCUSSION

In this paper a complete set of sequence-specific ^1H-resonance assignments has been presented for the polypeptide ATX III and its solution properties have been characterized. The n.m.r. results indicate that ATX III adopts a stable tertiary structure in aqueous solution, which consists primarily of a network of reverse turns.

A significant feature of the solution properties of ATX III is its strong tendency to aggregate at concentrations suitable for n.m.r. studies. Preliminary analytical ultracentrifugation studies indicate that association extends at least to the formation of a trimer at the highest concentrations used in our n.m.r. studies. It appears that electrostatic- and/or hydrogen-bonding interactions involving a carboxyl group contribute to aggregation. Hydrophobic interactions also play an important role, as the aromatic rings of both tryptophan residues and Tyr-7 are affected, with the aromatic resonances of Tyr-7 being extremely sensitive to concentration even at low pH.

The exchange rates found for the most slowly exchanging backbone amides of ATX III are similar to those found for polypeptides under similar conditions, such as apamin (18 residues; Bystrov et al., 1978) and the scorpion neurotoxin I_5A (35 residues; Arseniev et al., 1984), but significantly higher than those for small, stable proteins such as bovine pancreatic trypsin inhibitor (Wüthrich, 1986). This indicates that the conformational stability of ATX III is typical of polypeptides of comparable size and degree of disulphide cross-linking.

It is of interest to compare the structural information derived herein from n.m.r. data with inferences drawn previously about the secondary structure from c.d. studies and predictive algorithms. Using c.d., Ash et al. (1981) concluded that ATX III contains no α-helix and that its structure was stable over the pH range 1.8–12.0, both of which agree with the n.m.r. data presented here. They also found that one or both tryptophan residues was affected by a carboxyl ionization, which concurs with our observations regarding Trp-13. By contrast, their finding that neither tyrosine residue ionizes at high pH is inconsistent with the n.m.r. data. A model of the structure of ATX III was proposed by Smythies (1981) on the basis of a Chou–Fasman analysis. Although the amino-acid sequence used had the order of Cys-22 and Ser-23 inverted, the overall conclusion of this prediction, that ATX III consists of a nearly continuous series of β-turns, is borne out by our experimental data. According to this predicted structure, however, only one set of disulphide connectivities would be possible, i.e. 3–22, 4–17 and 6–11. These do not concur with the pairings suggested by the nOe connectivities.

The results presented in this paper provide the most detailed picture of the structure of ATX III to date. Nevertheless, a complete tertiary structure of the molecule is required in order to understand the molecular basis for its activity, and this is currently being determined from n.m.r. data. Normally, tertiary-structure determination would be straightforward for a molecule the size of ATX III, but in this case the procedure is complicated by uncertainty with respect to the locations of the disulphide bonds and by the effects of aggregation. To address the latter

problem, spectra have to be recorded at increasing dilutions to identify and exclude all nOe connectivities arising from intermolecular contacts in the aggregate. Analytical ultracentrifugation experiments are also being carried out in order to characterize the nature of the aggregation. Once a set of uniquely intramolecular constraints has been determined, a series of structure calculations can be carried out with different disulphide pairings in order to establish which is correct. When the final structure is available, it will be of interest to compare its molecular surface with those of the sea anemone and scorpion proteins that bind to the same receptor site on the sodium channel, and to correlate the structure with the results of limited chemical-modification studies on ATX III (Beress, 1979). At this stage it appears that ATX III lacks a disordered loop of the type found in the structures of the longer sea anemone toxins (46–49 residues) and which is known to contain several residues essential for biological activity (Norton, 1991). The structure will also allow us to identify those regions of the surface that participate in aggregation and then to evaluate the possibility that a dimer of ATX III might be the species that binds to the sodium channel.

This work was supported in part by grants from the Australian Research Council (R.S.N.) and the Deutsche Forschungsgemeinschaft (E.W.). We thank Nick Manoleras for helpful discussions and Dennis Hare for providing software.

REFERENCES

Arseniev, A. S., Kondakov, V. I., Maiorov, V. N. and Bystrov, V. F. (1984) FEBS Lett. **165**, 57–62

Ash, P., Hider, R. C., Menez, A. and Wunderer, G. (1981) Biochim. Biophys. Acta **669**, 231–235

Bahraoui, E. M., El Ayeb, M., Grainier, C., Beress, L. and Rochat, H. (1989) Eur. J. Biochem. **180**, 55–60

Barhanin, J., Hugues, M., Schweitz, H., Vincent, J.-P. and Lazdunski, M. (1981) J. Biol. Chem. **256**, 5764–5769

Bax, A. and Davis, D. G. (1985) J. Magn. Reson. **65**, 355–360

Beress, L. (1979) Habilitationschrift, Institut für Meereskunde an der Christian-Albrechts Universität, Kiel

Received 17 December 1992/10 February 1993; accepted 17 February 1993

Beress, L. (1982) Pure Appl. Chem. **54**, 1981–1994

Beress, L., Beress, R. and Wunderer, G. (1975) FEBS Lett. **50**, 311–314

Billeter, M., Braun, W. and Wüthrich, K. (1982) J. Mol. Biol. **155**, 321–346

Braunschweiler, L. and Ernst, R. R. (1983) J. Magn. Reson. **53**, 521–528

Bundi, A. and Wüthrich, K. (1979) Biopolymers **18**, 285–297

Bystrov, V. F., Arseniev, A. S. and Gavrilov, Y. D. (1978) J. Magn. Reson. **30**, 151–184

Catterall, W. A. (1988) Science **242**, 50–61

Chazin, W. J. and Wright, P. E. (1987) Biopolymers **29**, 973–977

Driscoll, P. C., Gronenborn, A. M., Beress, L. and Clore, G. M. (1989) Biochemistry **28**, 2188–2198

Fogh, R. H., Kem, W. R. and Norton, R. S. (1990) J. Biol. Chem. **265**, 13016–13028

Fontecilla-Camps, J. C., Habersetzer-Rochat, C. and Rochat, H. (1988) Proc. Natl. Acad. Sci. U.S.A. **85**, 7443–7447

Gould, A. R., Mabbutt, B. C. and Norton, R. S. (1990) Eur. J. Biochem. **189**, 145–153

Jeener, J., Meier, B. H. A., Bachmann, P. and Ernst, R. R. (1979) J. Chem. Phys. **71**, 4546–4553

Kem, W. R. (1988) in Biology of Nematocysts (Hessinger, D. and Lenhoff, H., eds.), pp. 375–405, Academic Press, New York

Kumar, N. V., Pease, J. H. B., Schweitz, H. and Wemmer, D. E. (1990) in Marine Toxins. Origin, Structure and Molecular Pharmacology (Hall, S. and Strichartz, G., eds.), pp. 290–303, Am. Chem. Soc., Washington

Levitt, M. H. and Freeman, R. (1979) J. Magn. Reson. **33**, 473–476

Llewellyn, L. E. and Norton, R. S. (1991) Biochem. Int. **24**, 937–946

Macura, S., Huang, Y., Suter, D. and Ernst, R. R. (1981) J. Magn. Reson. **43**, 259–281

Manoleras, N. and Norton, R. S. (1992) J. Biomol. NMR **2**, 485–494

Marion, D. and Wüthrich, K. (1983) Biochem. Biophys. Res. Commun. **113**, 967–974

Müller, N., Ernst, R. R. and Wüthrich, K. (1986) J. Am. Chem. Soc. **108**, 6482–6492

Nishida, S., Fujita, S., Warashina, A., Satake, M. and Tamiya, N. (1985) Eur. J. Biochem. **150**, 171–173

Norton, R. S. (1990) Aust. J. Biotechnol. **4**, 114–120

Norton, R. S. (1991) Toxicon **29**, 1051–1084

Piantini, U., Sørenson, O. W. and Ernst, R. R. (1982) J. Am. Chem. Soc. **104**, 6800–6801

Shaka, A. J. and Freeman, R. (1983) J. Magn. Reson. **51**, 169–173

Smythies, J. R. (1981) Med. Hypoth. **7**, 707–710

Torda, A. E., Mabbutt, B. C., van Gunsteren, W. F. and Norton, R. S. (1988) FEBS Lett. **239**, 266–270

van Geet, A. L. (1970) Anal. Chem. **42**, 679–680

Wagner, G. and Zuiderweg, E. R. P. (1983) Biochem. Biophys. Res. Commun. **113**, 854–860

Widmer, H., Billeter, M. and Wüthrich, K. (1989) Proteins **6**, 357–371

Wishart, D. S., Sykes, B. D. and Richards, F. M. (1992) Biochemistry **31**, 1647–1651

Wokaun, A. and Ernst, R. R. (1977) Chem. Phys. Lett. **52**, 407–412

Wüthrich, K. (1986) NMR of Proteins and Nucleic Acids, Wiley, New York